Insights on the limiting factors of $Cu_2ZnGeSe_4$ based solar cells

I. Anefnaf[a,b], S. Aazou[a,b,*], Y. Sánchez[c], P.Vidal-Fuentes [c], R. Fonoll-Rubio [c], K. J. Tiwari [c], S. Giraldo[c], Z. Jehl Li-Kao[d], M. Guc [c], E. Saucedo[d] and Z. Sekkat[a,b,e]

[a] Department of Chemistry, Faculty of Sciences, Mohammed V University in Rabat, Morocco
[b] Optics & Photonics Center, Moroccan Foundation for Advanced Science, Innovation and Research -MAScIR, Rabat, Morocco
[c] Catalonia Institute for Energy Research - IREC, Sant Adrià de Besòs, Barcelona, Spain
[d] Department Enginyeria Electrònica, Universitat Politècnica Catalunya (UPC), Barcelona, Spain
[e] Department of Applied Physics, Osaka University, 2-1 Yamadaoka, Suita, Osaka, Japan

Abstract:

Germanium-based wide band gap Kesterite semiconductor $Cu_2ZnGe(S,Se)_4$ (CZGeSSe) is considered a very promising absorber compound as top cell in tandem devices. Autonomy to tailor the band gap from ~1.47 eV ($Cu_2ZnGeSe_4$-CZGeSe) to ~2.2 eV (Cu_2ZnGeS_4-CZGeS), as well as non-toxic constituents makes this compound a strong candidate for further scientific exploration. However, the record efficiency of $Cu_2ZnGeSe_4$ solar cells is still significantly lower than those of its predecessors $Cu_2ZnSn(S_xSe_{1-x})_4$ (CZTSSe), $Cu(In,Ga)Se_2$ (CIGS) and CdTe thin-film solar cells.

The comprehensive understanding of the factors limiting the performance of $Cu_2ZnGeSe_4$-based solar cells is the purpose of this work, by combining a complete characterization of the morphological, structural, compositional and optoelectronic properties of $Cu_2ZnGeSe_4$ absorbers and devices. Besides, an in-depth investigation of the main limitations is carried out, specifically focusing on studying the origin of the large V_{OC} deficit, the main recombination mechanisms, electric transport properties, band tails and possible $Cu_2ZnGeSe_4$/CdS band offset effects. The champion CZGeSe solar cell device reported in this work shows an efficiency of 6.42%, V_{oc} of 606 mV, J_{SC} of 17.77mA/cm^2 and FF of 59.65%. The results presented here demonstrate that the large voltage deficit of CZGeSe solar cells could be mainly ascribed to a Fermi level pinning at the interface, and modifications of the buffer layer to induce a "spike" at the pn junction could be beneficial. Additionally, low carrier diffusion lengths and lifetimes, along with possible back contact recombination, are identified as the main culprits for the limited carrier collection for low-energy photons. Finally, some strategies are proposed to face and overcome most of these issues and to help improving the CZGeSe performance.

1. INTRODUCTION

$Cu_2ZnSn(S_xSe_{1-x})_4$ (CZTSSe) is a promising candidate for thin-film photovoltaic applications[1], thanks to their advantageous properties including its ideal direct bandgap that can be tuned between 1.0 eV and 1.5 eV, high absorption coefficient (~10^4 cm^{-1}) and non toxicity make it suitable for solar cell application (single and tandem solar cells)[2–6]. However, the best reported efficiency, so far, for CZTSSe is 12.6% with bandgap energy of E_g=1.13 eV[7], which is about half of the efficiency of the close-cousin CIGS-based solar cell and much lower than the theoretical Shockley-Quiesser limit for CZTSSe, (32.8%).[8] One of the focal challenges so far for CZTSSe based solar cells is the poor open circuit voltage (V_{OC}).[9–11] The maximum V_{OC} depends mostly on the absorber bandgap but can be strongly affected in case of high recombination or defects pinning the Fermi level. Thus, to compare absorbers with different bandgap, the so called V_{OC}-deficit is introduced, defined as E_g/q-V_{OC} (where E_g is the absorber bandgap energy, V_{OC} is the open circuit voltage and q is the electron charge) and offering a figure of comparison between materials of different bandgaps, and it is around 0.6 eV for the record CZTSSe based solar cell.[7] Some studies identify that the main culprits for the large V_{OC} deficit are the intrinsic defects and the band tail.[12–14] Furthermore, several causes for the large V_{OC} deficit are suggested: (i) the disordering and lattice defects are acting as an effective recombination centers, and are resulting from the CZTSSe nature, including anti-sites (e.g., Sn_{Cu}, Sn_{Zn}), vacancies (e.g., V_{Zn}, V_{Sn}) and interstitial (e.g., Zn_i) defects in te system.[15,16] Particularly, the anti-site defects (Cu_{Zn} and Zn_{Cu}) are almost unavoidable in CZTSSe compound due to the similar ionic radius of Cu and Zn as well as their chemical properties.[17,18] (ii) the tail state formation which is ascribed to high defect concentrations producing electrostatic potential fluctuations[19–21] or spatial variations in the crystalline system and/or composition, driving to a nanoscale bandgap fluctuations.[22–24] (iii) the non-ideal band alignment between the absorber and the CdS, possibly causing high recombination at the absorber/CdS interface and hampering minority carrier transport.[25,26] There is a particular research axis targeting the reduction of defect density to boost device performance by optimizing processes of surface and grain boundary passivation[27–29]. Additionally, the issues of optical losses[30], anti-reflection coating and bulk CZTSSe quality[31] are also regularly addressed by the community. Nevertheless, the intrinsic point defects are still a critical issue in the bulk absorber.[32] The alternative solution to decrease cation disorder in CZTSSe compound is the cationic substitution: Zn with Cd,[33] Zn with Ba[34], Cu with Ag[35,36] and Sn with Ge.[37,38] IREC group[38,39] proved that partial substitution of Sn with Ge led to a performance enhancement of these thin film solar cells compared to their previous baseline cells. The crystalline quality and grain size were particularly improved, thus boosting the V_{OC}. Table 1 shows a summary of some successful studies introducing Ge in the CZTSSe solar cells. A significant improvement in the cell's voltage is obtained from very small quantities <0.005% (doping) up to around 40% (substitution of Sn with Ge).

Table 1 Summary of the beneficial effects of Ge on thin films kesterite solar cells.

Technique	Ge/Ge+Sn	Eff. (%)	FF(%)	J_{SC} (mA/cm^2)	V_{OC} (V)	Eg (eV)	V_{OC}-deficit [a] (V)	Ref
Molecular precursor solutions	0.25	11.0	33.6	33.6	583	1.15	0.31	40
Nanocrystal inks printing	0.30	9.4	63.8	31.9	460	1.19	0.48	41
DC Sputtering	< 0.005	11.8	66.3	38.3	463	1.04	0.31	37
DC Sputtering	< 0.005	10.6	66.7	33.6	473	1.05	0.30	42
DC Sputtering	< 0.005	10.1	66.8	33.6	453	1.04	0.31	39
DC Sputtering	0.20	9.2	65.1	29.9	471	1.12	0.40	43
Co-evaporation	0.22	12.32	72.7	32.2	527	1.11	0.35	44
Co-evaporation	0.22	10.03	62.7	29.5	543	1.19	0.39	45
Technique	**Cu/Zn+Ge**	**Eff. (%)**	**FF (%)**	**J_{SC} (mA/cm^2)**	**V_{OC} (V)**	**Eg (eV)**	**V_{OC}-deficit [a] (V)**	**Ref**
Evaporation	1.0	5.5	46	16	744	1.4	0.58	46
Evaporation	0.9	7.6	58	22.8	558	1.36	0.58	47
DC Sputtering	1.0	6.5	60	19.6	556	1.45	0.58	48
Evaporation	0.9	8.5	55.7	24.4	625	1.39	0.55	49
DC Sputtering	0.67	6.42	59.65	17.77	606	1.47	0.51	This work

[a] respected to Shockley–Queisser limit (SQ), and calculated by the authors with the available data in the different references.

The best efficiency reported so far for pure Ge-kesterite (CZGeSe) thin film solar cell is 8.5%, using metallic stack precursors annealed under H_2Se gas.[49] The highest open circuit voltage V_{OC} reported so far for pure Ge-kesterite (CZGeSe) is 744 mV with an efficiency of 5.5%.[46] Research studies on pure Ge-kesterite devices could be benefits to broaden the spectrum of kesterite application, and specifically for efficient photovoltaic tandem solar cells in combination with Si or a narrow bandgap chalcogenide compound. There are still several limitations to overcome due to the scarcity of studies of Ge-compounds, comparatively rare when considering their Sn counterpart, besides the first studies recently published about physical and fundamental properties of Ge-compounds.[50,51] In this context, it is of prime importance to acquire deeper understanding of the defects existing in CZGeSe-based materials and comprehend the key factors limiting CZGeSe-based thin film solar cell performance to push up the CZGeSe solar cells efficiency to a more competitive level.

To the best of our knowledge, no previous studies investigating and identifying the defects and limitations for CZGeSe-based thin film solar cell are available. For that purpose, our work intent is to assess and unveil limitations on complete CZGeSe solar cells. In the present study, a complete analysis of morphological, structural and compositional characterization of the prepared CZGeSe thin film based solar cell is presented. The highest performance achieved in this study is 6.42%, with V_{OC} of 606 mV, J_{SC} of 17.77 mA/cm^2 and FF of 59.65%. Furthermore, a broad range of material characterizations provides valuable insights on the factor limiting state-of-the-art devices, and specifically on the defects and recombination mechanisms.

2. EXPERIMENTAL SECTION

Precursor deposition:

$Cu_2ZnGeSe_4$ thin-films are prepared by sequential deposition of Cu, Zn and Ge stack precursors by DC-magnetron sputtering (Alliance AC450), with the elemental layer stack order Cu/Zn/Ge onto Mo-coated soda-lime glass substrates, 750nm Mo is deposited by DC-magnetron sputtering. The absorber composition is selected to obtain Cu-poor and Zn-rich precursors (Cu/(Zn+Ge) = 0.67 and Zn/Ge = 1.07) as confirmed by XRF measurement.

Reactive annealing:

The optimized thermal annealing process to growth $Cu_2ZnGeSe_4$ absorbers is carried out in a dedicated tubular furnace using graphite box with 100 mg elemental Se and 5 mg of $GeSe_2$. The thermal treatment used consists of a two-step annealing process, first step at 330°C for 30 min, with 20 °C/min ramping, in Ar dynamic pressure (1.5 mbar), followed by a second step at 480°C for 15 min, 20 °C/min ramping, in Ar (1bar) static pressure.

Solar cells elaboration:

The solar cells are completed after etching the synthesized absorbers with KCN solution (2% w/v, 2min) to clean and remove the secondary phases. Immediately after the chemical etching, ~50 nm of CdS is deposited by chemical bath deposition (CBD) from nitrate salts.[52] Then the transparent front electrode i-ZnO (50 nm) and In_2O_3:SnO_2 (ITO, 200 nm, 60Ω/sq) is deposited by DC-pulsed sputtering (Alliance Concept CT100). Finally, the solar cells are mechanically scribed (3×3 mm^2) with a microdiamond scriber (OEG MR200). Neither antireflective coating nor metallic grids are used for the optoelectronic characterization of the fabricated devices.

Films and devices characterization:

The composition and precursor thicknesses is characterized by using X-ray fluorescence (XRF) system (Fischercope XDV) previously calibrated by inductively coupled plasma mass spectrometry (ICP). The scanning electron microscope (SEM) micrographs are acquired with a ZEISS Series Auriga microscope using an acceleration voltage of 5 kV. Raman scattering spectra are performed by FHR 640 and iHR 320 monochromators from Horiba Jobin Yvon both coupled with CCD detectors. The first system is previously optimized for UV-visible spectral range and used with 442 nm and 532 nm excitation wavelengths. The second system is optimized for NIR range and used with 785 nm excitation wavelength. The lasers power densities are in the range 100-150 Wcm^{-2}. The characterizations are performed in a backscattering configuration though probe designed at IREC. Moreover, the in-depth chemical composition profiles of -Ge-kesterite absorber layer is investigated by Glow Discharge Optical Emission Spectroscopy (GDOES) using Horiba Jobin Yvon GD Profiler

2 spectrometer with 4 mm anode diameter. J-V measurements are performed on the completed devices using a calibrated Sun 3000 class AAA solar simulator (Abet Technologies, 25°C, AM1.5G illumination). The EQE spectra of the elaborated solar cells are measured by Bentham PVE300 system calibrated with Si and Ge photodiodes. The capacitance-voltage measurements are done in the dark, at room temperature with a modulation voltage of 50 mV with a Novocontrol Technologies impedance analyzer. J–V–T measurements are performed by a cryostat (Cold-Head model RDK-101D Sumitomo Heavy Industries Ltd.) cooled by helium closed cycle compressor (Zephyr HC-4A from Sumitomo cryogenics).

3. RESULTS AND DISCUSSION

The SEM micrographs of $Cu_2ZnGeSe_4$-based solar cells with the following configuration SLG/Mo/ $Cu_2ZnGeSe_4$/CdS/i-ZnO/ITO are investigated. The cross section of the entire $Cu_2ZnGeSe_4$ solar cell, as well as the top view of the absorber surface are presented in Figure 1. The top surface image of the absorber reveals large and closely packed grains well connected with each other's. The cross sectional image of the full device (after chemical etchings and CdS/TCO deposition) indicates large grains in the bulk extending throughout the whole thickness. Unlike CZTSe, CZGeSe seems to not (or just slightly) form the typical bilayer structure, with very few small crystals segregating at the back. In this sense, the cross sectional morphology of CZGeSe appears much better than CZTSe. The average absorber thickness is around 1.45 µm. However, it is very difficult to define the exact thickness of $MoSe_2$ phase, most probably due to their very thin nature related to the lower temperatures required for the synthesis of CZGeSe when compared with CZTSe (480 ºV vs 550 ºC respectively).

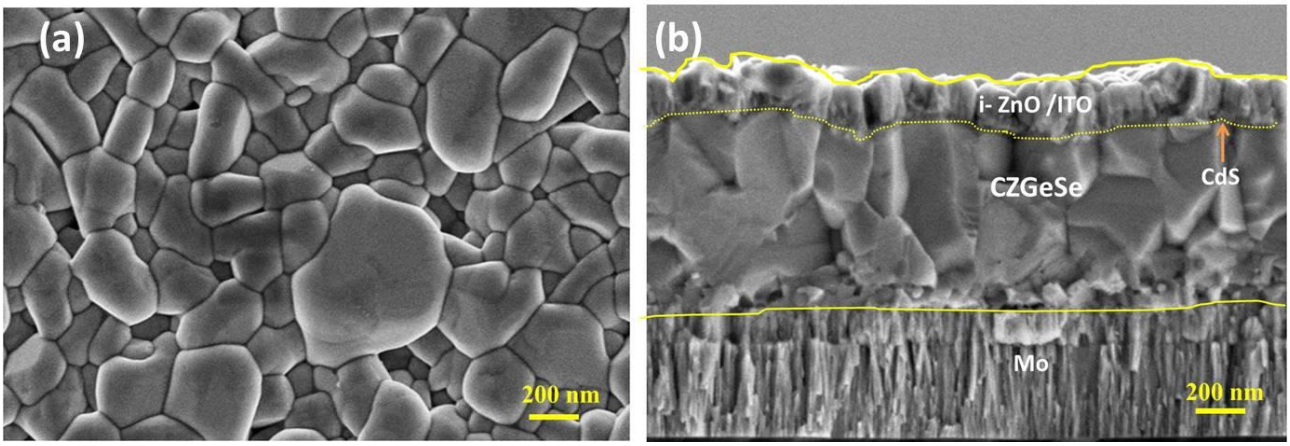

Fig. 1. *SEM micrographs of the $Cu_2ZnGeSe_4$ (a) top surface of the absorber and (b) Cross-section of the SLG/Mo/ $Cu_2ZnGeSe_4$/CdS/i-ZnO/ITO.*

The Raman scattering spectra are measured under different excitation conditions to check the presence of any secondary phases. Analysis of the obtained spectra (Figure 2) showed presence of $Cu_2ZnGeSe_4$ related peaks only.[53] A narrow width of the Raman peaks corresponds to the high crystalline quality of the absorber surface, an observation consistent with the aforementioned SEM images (Figure 1). Once again, this suggests that secondary phases are less prone to be formed in this system than in CZTSe, suggesting a clear advantage of the Ge-compound. However, additional characterization using X-Ray Diffraction spectroscopy would be needed to assess with certainty the phase purity of the film. In that context, the comparatively lower efficiency of $Cu_2ZnGeSe_4$ solar cells may not be ascribed to morphological or phase-composition issues, as both appear fully compatible with high efficiency devices.

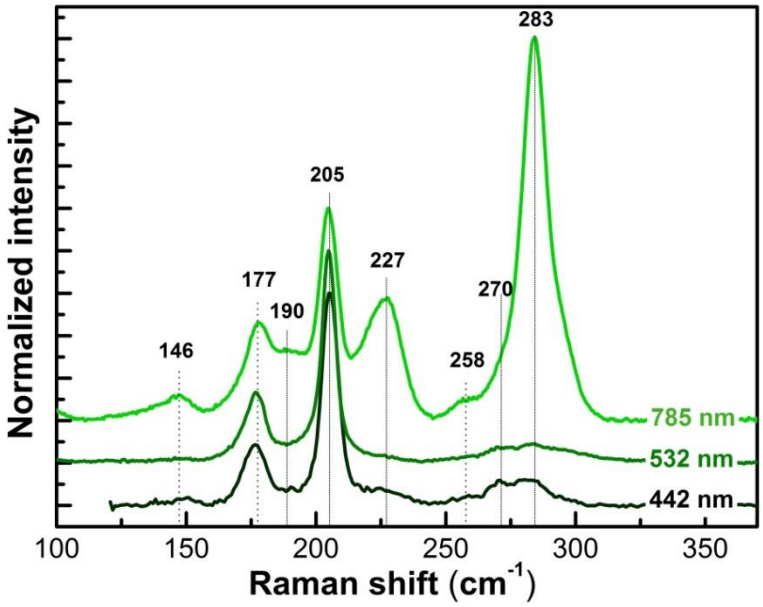

Fig. 2. *Raman scattering spectra of $Cu_2ZnGeSe_4$ based device measured under different excitation conditions. Numbers indicate the peaks position.*

One can notice that from the glow discharge optical emission spectroscopy (GDOES) profiles of Cu, Zn, Ge, Se and Mo (Figure 3), the cation distribution is relatively uniform at the top half of the absorber, whereas Cu tends to decrease and Ge to slightly increase (as compared to the other elements) towards the back region of the absorber. This can suggest that Ge-rich phases are accumulated towards the back region, as it is proven in this system where Ge tends to naturally be present with higher concentration at the back area.[54] In such case, some secondary phases can be expected at the back and affect the device performance (mainly the J_{SC} and the FF). Additionally, the combined decrease in Cu and Se composition toward the back interface could be ascribed to the presence of Cu-based secondary phases, though further material analysis (see Raman) do not allow

to conclude in that regard. A future XRD analysis would shed light on that question, though the $CuGeSe_3$ secondary phase appears to be the likeliest in that context.

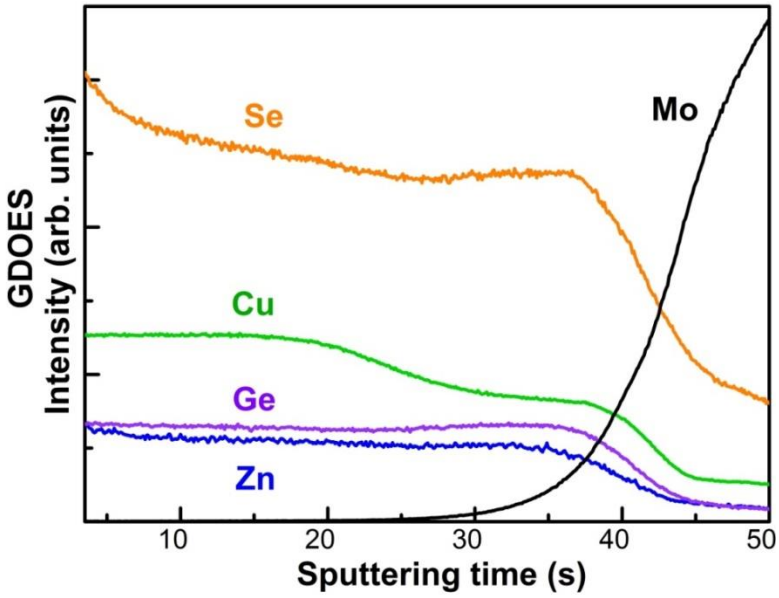

Fig. 3. *Depth composition profiles of $Cu_2ZnGeSe_4$ device performed by a glow discharge optical emission spectrometry analysis (GDOES).*

To further analyze the best device, the current density-voltage (J-V) characteristics and EQE measurement are performed. The device reveals a 6.42 % efficiency with a V_{OC} of 606 mV (Figure 4(a)), it is very important to highlight that neither anti-reflection coating nor metallic grid are used in this work. The optoelectronic parameters of the device are summarized in Table 2. J-V curves exhibit a distinct cross-over between dark and light characteristics (Figure 4(a)), which is often related to defect states at the CZGeSe/CdS interface or in the bulk of CdS layer, and leads to acceptor-like buffer traps states.[52] In order to get a deeper insight how to reduce defects and boost device performance, EQE measurement are presented Figure 4(b). In the region 300–500 nm, the collection losses are affected by parasitic absorption from the CdS/TCO. The EQE spectrum reaches a maximum close to 80% at 500 nm, showing that photocarriers generated close to the pn junction are efficiently collected and the p-n interface does not appear to be limiting the current; in the red and the infrared region however, the collection efficiency collapses, indicating either bulk recombination (low carrier diffusion length), incomplete absorption or back contact recombination. Incomplete absorption can be discarded in the largest part of the considered spectral range; indeed, the film's thickness is close to 1.5 μm, which is more than enough for complete absorption considering an absorption coefficient in the range of $10^{4\text{-}5}$. Hence, a low minority carrier diffusion length or back interface recombination appear to significantly hamper the collection of carriers generated deeper in the absorber. As the

morphology or the phase purity of CZGeSe appear excellent in both the SEM and Raman analysis, bulk recombination and native defects existing in the material could be important factor limiting the performance of the device. From the EQE results, the optical band gap of CZGeSe is estimated from a Tauc plot (inset Figure 4(b)), and it is found to be 1.47 eV.

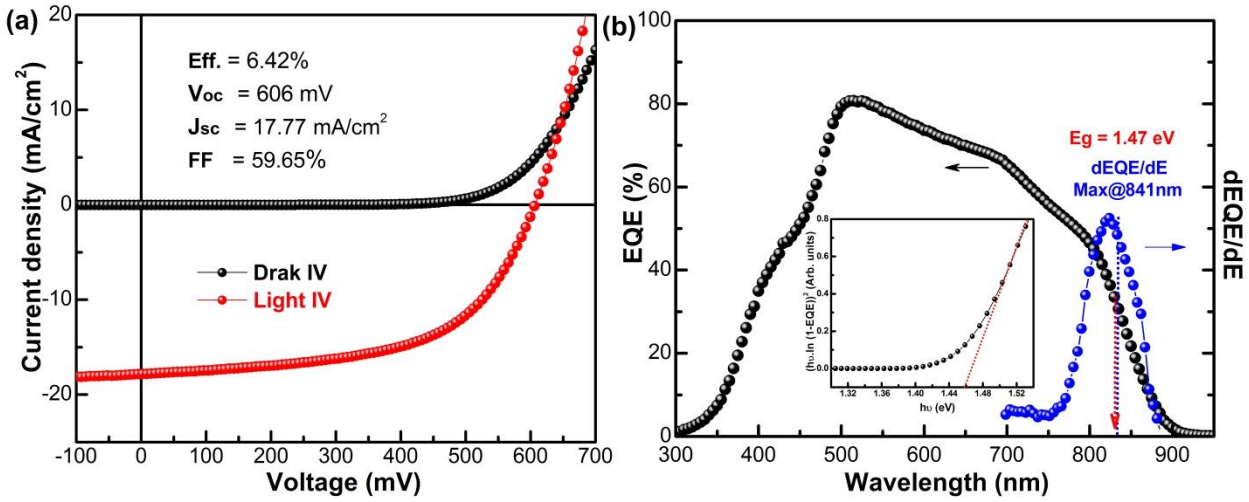

Fig. 4. *J-V characteristics (a) and EQE spectrum with the inset graph shows the band gap extraction by plotting* $(h\upsilon.\ln(1\text{-}EQE))^2$ *vs. energy of* $Cu_2ZnGeSe_4$ *(b).*

To understand further the $Cu_2ZnGeSe_4$ absorber nature, the device is measured by C-V characterization under 5.6 KHz. The carrier concentration and the depletion region width are calculated from capacitance–voltage (C-V) profile measured at room temperature (RT) on $Cu_2ZnGeSe_4$ device. Figure 5 displays the charge carrier versus the distance to the front interface (N_{CV} (x)). This later is calculated from C-V measurement of the solar cell and can include contributions of superficial and deep defects. The profile demonstrated in Figure 5 reveals a distinct U-shape, this profile was previously attributed to deep defects, interface defects and/or back contact barriers effects[55–57]. Moreover, the lowest value of U-shape can be taken as an approximation of the charge density. The carrier concentration reflects the properties of $Cu_2ZnGeSe_4$ near depletion region is of 1.7. 10^{15} cm^{-3} and a charge space region width (SCR) of 311 nm. This carrier concentration is at least one order of magnitude lower than the one reported typically in high efficiency CZTSe devices, indicating that $Cu_2ZnGeSe_4$ doping is not as easy. In fact, this lower carrier concentration can explain at least in part the reduction of the V_{OC}.

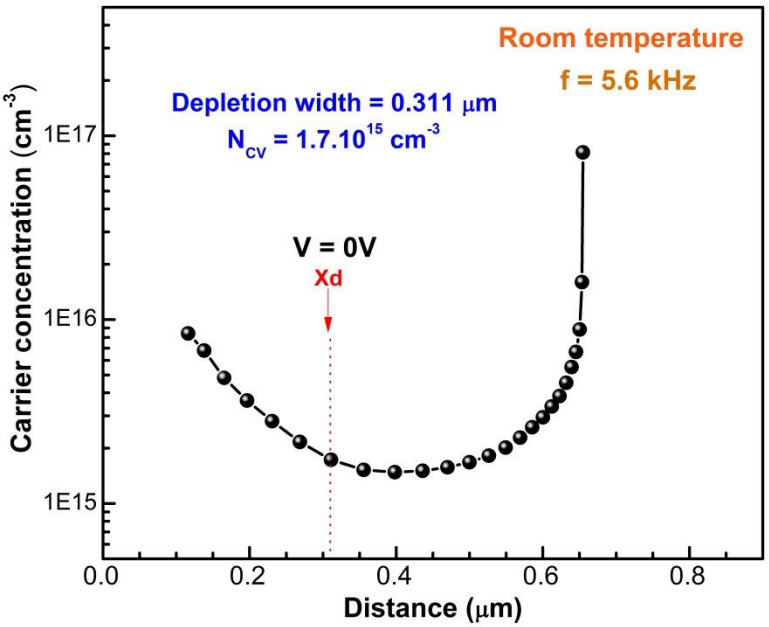

Fig. 5. *Charge carrier density versus the distance to the junction interface extracted from Capacitance-Voltage measurements of a $Cu_2ZnGeSe_4$ device.*

Table 2. *Summary of the optoelectronic parameters obtained for the best device presented in this work.*

Parameters	*Value*	*Units*
Eff.	6.5	%
V_{OC}	606	mV
J_{SC}	17.8	mA/cm^2
FF	59.6	%
SQ, V_{oc} deficit	0.51	V
V_{oc} deficit	0.81	V
R_S	0.14	Ω. cm^2
R_{sh}	8700	Ω. cm^2
J_0	1.6.10^{-4}	mA. cm^{-2}
A	1.7	--
Carrier concentration	1.7.10^{15}	cm^{-3}
SCR	310	nm
E_g	1.47	eV
E_U	22	eV
Ext. V_{oc} (0 K)	0.94	eV

Table 2 shows a summary of the determined optoelectronic parameters from the J–V characteristics, EQE, temperature-dependent V_{OC} and C–V measurements. The following information on the figures of merit (Figures 4–7) of the fabricated solar cell could be obtained from:

Open-circuit voltage (V_{OC}): The estimated built-in potential between the CdS and the absorber is 800mV, as shown on the simulated band diagram (Figure […] supplementary materials). The results reveal a V_{OC} of 606 mV and is very close to that of the record cell[49] (Table 1). The calculated V_{OC} deficit remains however high and can be considered as the main factor limiting the device efficiency. This high value might be attributed either to Fermi level pinning, and/or to intrinsic point defects. According to reference[58], the CdS and the $CuZnGeSe_2$ have no conduction band offset; while this is theoretically the most favorable case, the presence of interface defects can often lead to reduced performances a small spike-like interface as in the CIGSe/CdS is preferable. Hence, it is possible that interface defects are a limiting factor in our case, specifically through the pinning of the quasi-Fermi level reducing the cell's voltage; the effect of a Fermi level pinning at the pn interface is illustrated in Figure […] in the supplementary information, with a clear decrease of the voltage above an interface defect density threshold while the current remains unaffected. The V_{OC}-deficit compared to the Schockley Queisser limit (SQ) is estimated at ~0.51 V for the CZGeSe solar cell.

Short-circuit current density (J_{SC}): the device has a J_{SC} of 17.77 mA/ cm^2, which is still lower than CZTSe recorded device.[59,60] This lower value of J_{SC} was discussed when commenting the EQE, and is attributed to a poor collection of photocarriers generated by low energy photons (deeper in the absorber) due to a limited carrier diffusion length or back contact recombination.

Fill factor (FF): our best device achieved a FF of 59.65%, and is to our knowledge the highest value reported for this class of material (Table 1).[49] This high value indicates the formation of a relatively good CdS/CZGeSe interface in terms of carrier collection, which is consistent with our conclusion from the EQE curve.

As for the other parameters extracted from the fitting of the dark J-V characteristics using a single diode model, the reverse saturation current density (J_0) can be considered more or less in the range compared to CZTSSe ($7.\ 10^{-5}$ mA/cm^{-2})[7] and higher than CIGSe ($8.3.10^{-5}$ mA/cm^{-2})[61], which indicates a higher recombination rate.[62] Concerning the diode ideality factor (n), it remains below 2 (~1.703) suggesting that the device's current is limited by only one type of non-radiative recombination, which we believe takes place in the bulk as previously discussed.

To further investigate the origin of the losses in the device, bias dependent Internal Quantum Efficiency (IQE) was carried out to investigate the collection mechanisms in the device; the results are presented Figure 6(a) and compared with the previously described EQE curve. As shown Figure 6(a), the non-polarized EQE and IQE yield an integrated J_{SC} of 16.76 mA/cm^2 and 18.83 mA/cm^2 respectively. This integrated J_{SC} difference of 2.07 mA/cm^{-2} would translate to an efficiency of 6.81% if a perfect antireflective coating was used. We previously mentioned that carriers generated in the 600-950 nm spectral range are outside of the depletion width (W_d) and thus rely on diffusion for

collection without the assistance of a drift electric field. It is admitted that a large W_d can facilitate the collection of minority charges carriers inside the bulk of the absorber.[63] To further enlarge the depletion width of the device, a reverse bias voltage of (-1.0V) is applied to the device during the EQE measurements. From the results presented in Figure 6(a), comparing reverse bias voltage IQE measurement with the unbiased IQE, one can notice that the device shows an improvement in the photo-generated charge carrier for long wavelengths specifically (for reverse bias of -1.0V), leading to an enhancement in the IQE signal.

The ratio of the -1.0 V reverse bias voltage IQE and the unbiased-IQE response (0V) reveals the influence of the SCR width on the charges collection. As presented Figure 6(b), the ratio increases for longer wavelength, which confirms our hypothesis that carriers generated outside of the space charge region are not collected efficiently. It is therefore possible that the minority carrier diffusion length is insufficient in our $Cu_2ZnGeSe_4$ film, thus limiting the performance of the device. An alternative explanation relates to back contact recombination, as no specific passivation of the back interface is used in those devices. This would also align well with the hypothesized presence of secondary phases segregating at the back side of the film. In future experiments, increasing the absorber thickness will allow to discriminate between both suppositions, as back recombination would become irrelevant above a sufficient absorber thickness. Additionally, conduction band engineering strategies may allow to improve carrier collection outside of the space charge region by assisting the diffusion current with a drift component.

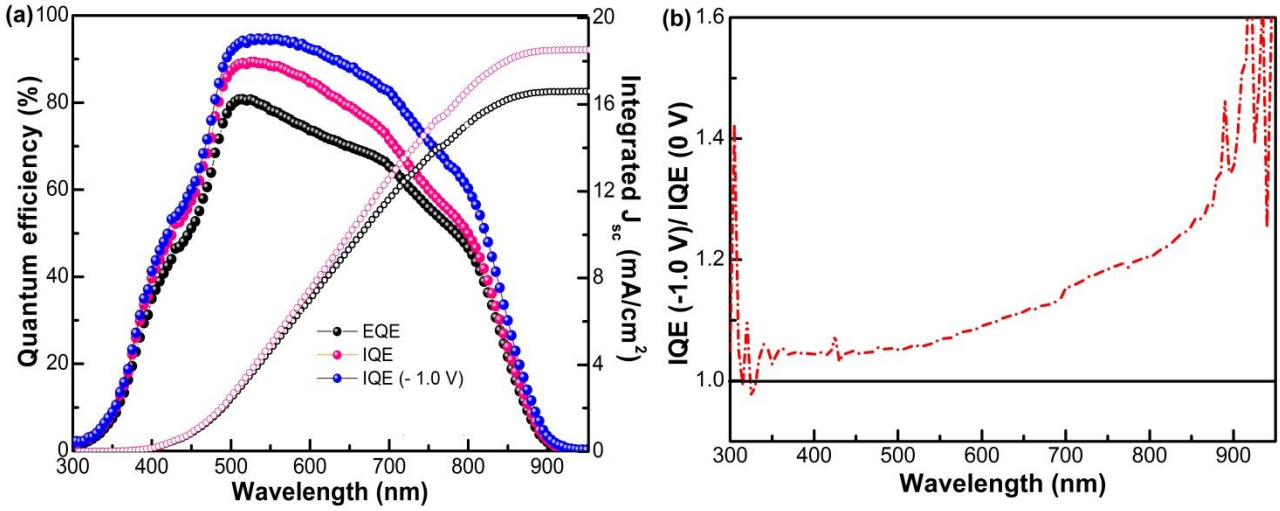

Fig. 6. *Response of the spectral characterization of the CZGeSe device: (a) external, internal, and biased internal (reverse at -1.0 V) quantum efficiency, the integrated J_{SC} estimated from EQE (black cycles) and IQE (pink cycles) and (b) IQE (-1.0 V)/IQE (0V) ratios.*

To further analyze the band tailing of the device, the Urbach energy (E_U) is estimated from the IQE as presented in equations[64] (3):

$$\alpha(h\nu) = \begin{cases} A_0\sqrt{\frac{E_U}{2\exp(1)}}\exp\left(\frac{h\nu - E_G}{E_U}\right) & \text{for } h\nu < E_G + \frac{E_U}{2} \\ A_0\sqrt{h\nu - E_G} & \text{for } h\nu \geq E_G + \frac{E_U}{2} \end{cases} \quad (3)$$

According to equation (3), an inverse slope between ln (1-IQE) in the long wavelength edge and hυ gives the E_U. From the linearization of equation (3), equivalent to the y-axis on Figure 7, the E_U value extracted as the inverse of the slope of the linear fit on the region E-Eg < 0; Urbach energy (E_U) in semiconductors is defined as the width of the Urbach tail. Urbach tail model and EQE fitting give band tailing Urbach energy parameter E_U of ~22 meV. According to reference [REF], an Urbach energy above 20meV is the threshold for a high voltage deficit while it does not have a direct relation to the current. This observation is consistent with the previously developed hypothesis that interface defects, in our case, are primarily a detriment to the voltage rather than the current, which also aligns well with the model's result shown in the supplementary information. It is important to highlight that the estimated E_U value in this work is smaller compared with the previously reported one for a similar absorber CZGeSe with a value of ~28 meV.[65] An E_U of about 33 meV is moreover reported for the record CZTGSe device.[44] However, the E_U value for Sn-kesterite is estimated to be ~60 meV for CZTSSe[66], and 70 meV for CZTS.[67] Values in the range of 30meV are reported for the best CZTSe devices [REF]. Hence, this comparison tends to indicate that the substitution of Sn by Ge in kesterite solar cells can possibly benefit in reducing the crystalline disorder resulting in an Urbach tails drop, which is consistent with the previously discussed high crystalline quality.

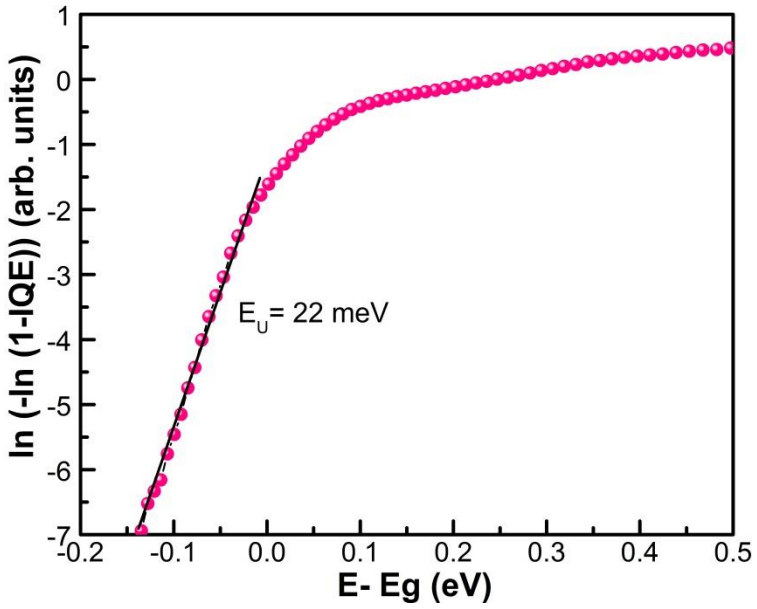

Fig. 7. *Urbach energy extracted from IQE of the $Cu_2ZnGeSe_4$ device.*

The V_{OC} deficit issues could thus be attributed to a combination of bulk defects and Fermi level pinning at the pn interface at room temperature (RT). Discriminating between both hypotheses would require a more advanced electrical characterization, and specifically a temperature dependent admittance spectroscopy analysis [REF Kobayashi]. While of major interest, such study is beyond the current scope of this work and may be tackled in future investigations. A basic numerical modeling of an equivalent solar cell structure (showed Figure […] in the supplementary materials) reveals that above a certain defect density threshold, interface defects will indeed pin the Fermi level and severely hamper the voltage of the solar cell. To gain additional insights on this limitation, temperature dependent J−V is carried out for the CZGeSe device (Figure 8). The V_{OC} is associated to the temperature T as follows[68]:

$$V_{OC} = \frac{E_A}{q} - \frac{AkT}{q} ln\left(\frac{J_{00}}{J_{SC}}\right) \qquad (4)$$

Where E_A is the activation energy of the dominant defect, A is the diode ideality factor, k is the Boltzmann constant, J_{00} is the reverse saturation current pre-factor and J_{SC} is the short circuit current density. Following relation (4), the V_{OC} is linearly related to the temperature, and the V_{OC} extrapolation at 0K yields the E_A. An activation energy of 940mV is calculated, significantly lower than the bandgap value of the film. Following an interpretation similar to reference [72], such value can be ascribed to a voltage limitation at the buffer/absorber interface; as we previously established that no significant conduction band offset exists in our devices, this limitation is thus consistent with a defect-related pinning of the Fermi level at the pn interface. A more detailed admittance spectroscopy analysis would be needed for unequivocally conclude on that matter.

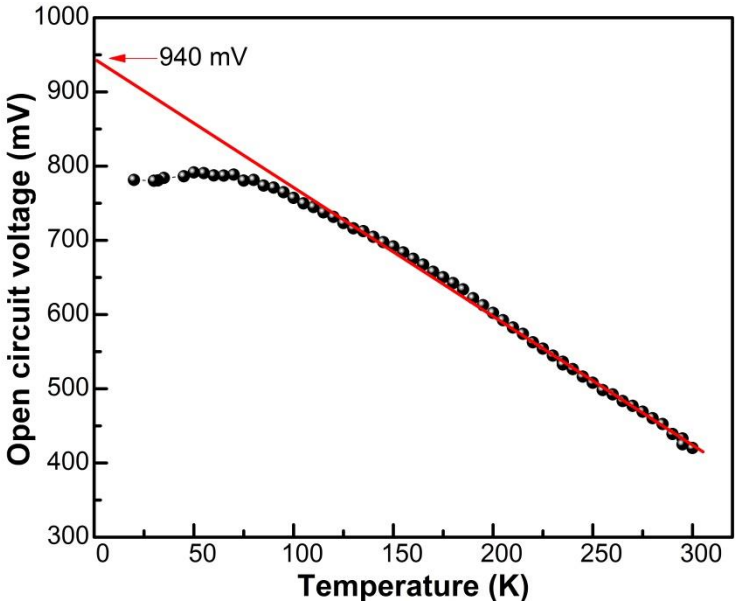

Fig. 7. *Temperature dependence of V_{OC} of the device with data extrapolated to 0K to extract the activation energy (E_a) of the recombination mechanism.*

Conclusion

The present work demonstrates the feasibility of synthesizing PV-quality $Cu_2ZnGeSe_4$ absorbers using a deposition of Cu/Zn/Ge metallic stack precursors by DC-magnetron sputtering technique, and then selenized through a reactive annealing. The champion solar cell device presented in this work shows a PCE of 6.42%, FF of 59.65%, V_{OC} of 606 mV, and J_{sc} of 17.77 mA/cm^2.

This work paves the way towards a better identification and understanding of the factors limiting $Cu_2ZnGeSe_4$ solar cells performance.

The following conclusions are drawn from our study:

- The large V_{OC} deficit can likely be ascribed to a Fermi level pinning at the interface, though the influence of bulk defects shouldn't be yet discarded. A spike-like absorber/buffer junction could alleviate this issue.
- The EQE analysis and the ratio between IQE(0V) and IQE(-1V) demonstrate that carriers generated outside of the depletion region are not efficiently collected, which we believe is related to a limited minority carrier diffusion length in the CZGeSe film or back contact recombination. While we believe that a defect state is pinning the Fermi level at the pn interface, it is unlikely that this defect participates to the current limitation as the EQE exceeds 80% in the low wavelength / high-energy range.
- A high crystalline quality is obtained, confirmed by SEM observation, Raman analysis, and the comparatively low Urbach energy (E_U = 22 meV).

To further improve the devices presented in this work, several strategies could be followed. The Cu content of the films presented in this study is comparatively low in regard to the literature of the field. While this value yielded the highest performance in our process, it is likely that optimizing absorbers with higher Cu content may be a pathway for efficiency increases. The use of alkali post-deposition treatments has demonstrated a spectacular improvement in the carrier lifetime in CIGSe solar cells, especially when using heavier elements such as Rb or Cs. A similar approach could be followed in $Cu_2ZnGeSe_4$ solar cells with a higher Cu content. Additionally, the buffer layer composition may also be positively altered by substituting a limited amount of Cd by Zn and obtain a spike-like pn interface, which could help alleviating the interface voltage limitation.

Declaration of competing interest

The authors declare that they have no known competing financial interests or personal relationships that could have appeared to influence the work reported in this paper.

Acknowledgments

We gratefully acknowledge the help provided by INFINITE-CELL project (H2020-MSCA RISE-2017 777968), by the Spanish Ministry of Science, Innovation, and Universities under the IGNITE (ENE2017-87671-C3-1-R), by the European Regional Development Funds (ERDF, FEDER Programa Competitivitat de Catalunya 2007–2013) and CERCA Programme/Generalitat de Catalunya. and the help carried out by the project PPR/2015/59 funded by the Moroccan Ministry of Higher Education and Research. Authors from IREC belong to the SEMS (Solar Energy Materials and Systems) Consolidated Research Group of the "Generalitat de Catalunya" (Ref. 2017 SGR 862).

References

1. Wong, L. H. *et al.* Emerging inorganic solar cell efficiency tables (Version 1). *J. Phys. Energy* **1**, 032001 (2019).
2. Guo, Q. *et al.* Fabrication of 7.2% Efficient CZTSSe Solar Cells Using CZTS Nanocrystals. *J. Am. Chem. Soc.* **132**, 17384–17386 (2010).
3. Liu, F. *et al.* Kesterite $Cu_2ZnSn(S,Se)_4$ Solar Cells with beyond 8% Efficiency by a Sol–Gel and Selenization Process. *ACS Appl. Mater. Interfaces* **7**, 14376–14383 (2015).
4. Bag, S. *et al.* Low band gap liquid-processed CZTSe solar cell with 10.1% efficiency. *Energy Environ. Sci.* **5**, 7060 (2012).
5. Wang, G. *et al.* Fabrication of a $Cu_2ZnSn(S,Se)_4$ Photovoltaic Device by a Low-Toxicity Ethanol Solution Process. *ACS Appl. Mater. Interfaces* **5**, 10042–10047 (2013).
6. Haass, S. G. *et al.* 11.2% Efficient Solution Processed Kesterite Solar Cell with a Low Voltage Deficit. *Adv. Energy Mater.* **5**, 1500712 (2015).
7. Wang, W. *et al.* Device characteristics of CZTSSe thin-film solar cells with 12.6% efficiency. *Adv. Energy Mater.* **4**, 1–5 (2014).
8. Siebentritt, S. Why are kesterite solar cells not 20% efficient? *Thin Solid Films* **535**, 1–4 (2013).
9. Kim, J., Park, S., Ryu, S., Oh, J. & Shin, B. Improving the open-circuit voltage of $Cu_2ZnSnSe_4$ thin film solar cells via interface passivation: Open-circuit voltage of $Cu_2ZnSnSe_4$ thin film solar cells. *Prog. Photovolt. Res. Appl.* **25**, 308–317 (2017).
10. Tai, K. F. Investigating the Open-Circuit Voltage Deficit in CZTSSe Solar Cells. (2015) doi:10.13140/RG.2.2.20153.98404.
11. Mitzi, D. B., Gunawan, O., Todorov, T. K., Wang, K. & Guha, S. The path towards a high-performance solution-processed kesterite solar cell. *Sol. Energy Mater. Sol. Cells* **95**, 1421–1436 (2011).

12. Gunawan, O., Gokmen, T. & Mitzi, D. B. Suns- V_{OC} characteristics of high performance kesterite solar cells. *J. Appl. Phys.* **116**, 084504 (2014).

13. Polizzotti, A., Repins, I. L., Noufi, R., Wei, S.-H. & Mitzi, D. B. The state and future prospects of kesterite photovoltaics. *Energy Environ. Sci.* **6**, 3171 (2013).

14. Mitzi, D. B., Gunawan, O., Todorov, T. K. & Barkhouse, D. A. R. Prospects and performance limitations for Cu–Zn–Sn–S–Se photovoltaic technology. *Philos. Trans. R. Soc. Math. Phys. Eng. Sci.* **371**, 20110432 (2013).

15. Chen, S., Walsh, A., Gong, X.-G. & Wei, S.-H. Classification of Lattice Defects in the Kesterite Cu_2ZnSnS_4 and $Cu_2ZnSnSe_4$ Earth-Abundant Solar Cell Absorbers. *Adv. Mater.* **25**, 1522–1539 (2013).

16. Giraldo, S. *et al.* Progress and Perspectives of Thin Film Kesterite Photovoltaic Technology: A Critical Review. *Adv. Mater.* **31**, 1806692 (2019).

17. Kattan, N. A., Griffiths, I. J., Cherns, D. & Fermín, D. J. Observation of antisite domain boundaries in Cu_2ZnSnS_4 by atomic-resolution transmission electron microscopy. *Nanoscale* **8**, 14369–14373 (2016).

18. Chen, S., Gong, X. G., Walsh, A. & Wei, S.-H. Defect physics of the kesterite thin-film solar cell absorber Cu2ZnSnS4. *Appl. Phys. Lett.* **96**, 021902 (2010).

19. Gokmen, T., Gunawan, O., Todorov, T. K. & Mitzi, D. B. Band tailing and efficiency limitation in kesterite solar cells. *Appl. Phys. Lett.* **103**, 103506 (2013).

20. Mendis, B. G. *et al.* The nature of electrostatic potential fluctuations in Cu_2ZnSnS_4 and their role on photovoltaic device performance. *J. Phys. Conf. Ser.* **471**, 012014 (2013).

21. Bishop, D. M. *et al.* Modification of defects and potential fluctuations in slow-cooled and quenched $Cu_2ZnSnSe_4$ single crystals. *J. Appl. Phys.* **121**, 065704 (2017).

22. Rey, G. *et al.* On the origin of band-tails in kesterite. *Sol. Energy Mater. Sol. Cells* **179**, 142–151 (2018).

23. Scragg, J. J. S. *et al.* Cu-Zn disorder and band gap fluctuations in $Cu_2ZnSn(S,Se)_4$: Theoretical and experimental investigations: Cu-Zn disorder and band gap fluctuations in $Cu_2ZnSn(S,Se)_4$. *Phys. Status Solidi B* **253**, 247–254 (2016).

24. Gunawan, O., Todorov, T. K. & Mitzi, D. B. Loss mechanisms in hydrazine-processed Cu2ZnSn(Se,S)4 solar cells. *Appl. Phys. Lett.* **97**, 233506 (2010).

25. Platzer-Björkman, C. *et al.* Reduced interface recombination in Cu_2ZnSnS_4 solar cells with atomic layer deposition $Zn_{1-x}Sn_xO_y$ buffer layers. *Appl. Phys. Lett.* **107**, 243904 (2015).

26. Yan, C. *et al.* Band alignments of different buffer layers (CdS, Zn(O,S), and In_2S_3) on Cu_2ZnSnS_4. *Appl. Phys. Lett.* **104**, 173901 (2014).

27. Xin, H. *et al.* Lithium-doping inverts the nanoscale electric field at the grain boundaries in $Cu_2ZnSn(S,Se)_4$ and increases photovoltaic efficiency. *Phys. Chem. Chem. Phys.* **17**, 23859–23866 (2015).

28. Courel, M., Andrade-Arvizu, J. A. & Vigil-Galán, O. Towards a CdS/Cu_2ZnSnS_4 solar cell efficiency improvement: A theoretical approach. *Appl. Phys. Lett.* **105**, 233501 (2014).

29. Kim, J. H. *et al.* Atomic-Scale Observation of Oxygen Substitution and Its Correlation with Hole-Transport Barriers in $Cu_2ZnSnSe_4$ Thin-Film Solar Cells. *Adv. Energy Mater.* **6**, 1501902 (2016).

30. Winkler, M. T. *et al.* Optical designs that improve the efficiency of $Cu_2ZnSn(S,Se)_4$ solar cells. *Energy Env. Sci* **7**, 1029–1036 (2014).

31. Tuan, D. A., Ke, N. H., Thi Kieu Loan, P. & Hung, L. V. T. A method to improve crystal quality of CZTSSe absorber layer. *J. Sol-Gel Sci. Technol.* **87**, 245–253 (2018).

32. Levcenko, S., Tezlevan, V. E., Arushanov, E., Schorr, S. & Unold, T. Free-to-bound recombination in near stoichiometric Cu 2 ZnSnS 4 single crystals. *Phys. Rev. B* **86**, (2012).

33. Su, Z. *et al.* Cation Substitution of Solution-Processed Cu_2ZnSnS_4 Thin Film Solar Cell with over 9% Efficiency. *Adv. Energy Mater.* **5**, 1500682 (2015).

34. Shin, D. *et al.* Earth-Abundant Chalcogenide Photovoltaic Devices with over 5% Efficiency Based on a $Cu_2BaSn(S,Se)_4$ Absorber. *Adv. Mater.* **29**, 1606945 (2017).

35. Gershon, T. *et al.* Photovoltaic Materials and Devices Based on the Alloyed Kesterite Absorber $(Ag_xCu_{1-x})_2ZnSnSe_4$. *Adv. Energy Mater.* **6**, 1502468 (2016).

36. Guchhait, A. *et al.* Enhancement of Open-Circuit Voltage of Solution-Processed Cu_2ZnSnS_4 Solar Cells with 7.2% Efficiency by Incorporation of Silver. *ACS Energy Lett.* **1**, 1256–1261 (2016).

37. Giraldo, S. *et al.* How small amounts of Ge modify the formation pathways and crystallization of kesterites. *Energy Environ. Sci.* **11**, 582–593 (2018).

38. Neuschitzer, M. *et al.* V_{oc} Boosting and Grain Growth Enhancing Ge-Doping Strategy for $Cu_2ZnSnSe_4$ Photovoltaic Absorbers. *J. Phys. Chem. C* **120**, 9661–9670 (2016).

39. Giraldo, S. *et al.* Large Efficiency Improvement in $Cu_2ZnSnSe_4$ Solar Cells by Introducing a Superficial Ge Nanolayer. *Adv. Energy Mater.* **5**, 1501070 (2015).

40. Collord, A. D. & Hillhouse, H. W. Germanium Alloyed Kesterite Solar Cells with Low Voltage Deficits. *Chem. Mater.* **28**, 2067–2073 (2016).

41. Hages, C. J. *et al.* Improved performance of Ge-alloyed CZTGeSSe thin-film solar cells through control of elemental losses: Improved performance of CZTGeSSe solar cells. *Prog. Photovolt. Res. Appl.* **23**, 376–384 (2015).

42. Giraldo, S. *et al.* $Cu_2ZnSnSe_4$ -Based Solar Cells With Efficiency Exceeding 10% by Adding a Superficial Ge Nanolayer: The Interaction Between Ge and Na. *IEEE J. Photovolt.* **6**, 754–759 (2016).

43. Andrade-Arvizu, J. *et al.* Rear Band gap Grading Strategies on Sn–Ge-Alloyed Kesterite Solar Cells. *ACS Appl. Energy Mater.* **3**, 10362–10375 (2020).

44. Kim, S., Kim, K. M., Tampo, H., Shibata, H. & Niki, S. Improvement of voltage deficit of Ge-incorporated kesterite solar cell with 12.3% conversion efficiency. *Appl. Phys. Express* **9**, 102301 (2016).

45. Kim, S. *et al.* Ge-incorporated Cu2ZnSnSe4 thin-film solar cells with efficiency greater than 10%. *Sol. Energy Mater. Sol. Cells* **144**, 488–492 (2016).

46. Sahayaraj, S. *et al.* Optoelectronic properties of thin film Cu2ZnGeSe4 solar cells. *Sol. Energy Mater. Sol. Cells* **171**, 136–141 (2017).

47. Choubrac, L. *et al.* 7.6% CZGSe Solar Cells Thanks to Optimized CdS Chemical Bath Deposition. *Phys. Status Solidi A* **215**, 1800043 (2018).

48. Benhaddou, N. *et al.* Uncovering details behind the formation mechanisms of $Cu_2ZnGeSe_4$ photovoltaic absorbers. *J. Mater. Chem. C* **8**, 4003–4011 (2020).

49. Choubrac, L. *et al.* Sn Substitution by Ge: Strategies to Overcome the Open-Circuit Voltage Deficit of Kesterite Solar Cells. *ACS Appl. Energy Mater.* **3**, 5830–5839 (2020).

50. Gunder, R., Márquez-Prieto, J. A., Gurieva, G., Unold, T. & Schorr, S. Structural characterization of off-stoichiometric kesterite-type $Cu_2ZnGeSe_4$ compound semiconductors: from cation distribution to intrinsic point defect density. *CrystEngComm* **20**, 1491–1498 (2018).

51. Courel, M., Sanchez, T. G., Mathews, N. R. & Mathew, X. Cu_2ZnGeS_4 thin films deposited by thermal evaporation: the impact of Ge concentration on physical properties. *J. Phys. Appl. Phys.* **51**, 095107 (2018).

52. Neuschitzer, M. *et al.* Optimization of CdS buffer layer for high-performance $Cu_2ZnSnSe_4$ solar cells and the effects of light soaking: elimination of crossover and red kink: CdS and effects of light soaking: elimination of crossover and red kink. *Prog. Photovolt. Res. Appl.* **23**, 1660–1667 (2015).

53. Guc, M. *et al.* Polarized Raman scattering analysis of $Cu_2ZnSnSe_4$ and $Cu_2ZnGeSe_4$ single crystals. *J. Appl. Phys.* **114**, 193514 (2013).

54. Márquez, J. *et al.* Chemistry and Dynamics of Ge in Kesterite: Toward Band-Gap-Graded Absorbers. *Chem. Mater.* **29**, 9399–9406 (2017).

55. Yin, L. *et al.* Limitation factors for the performance of kesterite Cu_2ZnSnS_4 thin film solar cells studied by defect characterization. *RSC Adv.* **5**, 40369–40374 (2015).

56. Li, J. V. *et al.* Theoretical analysis of effects of deep level, back contact, and absorber thickness on capacitance–voltage profiling of CdTe thin-film solar cells. *Sol. Energy Mater. Sol. Cells* **100**, 126–131 (2012).

57. Heath, J. T., Cohen, J. D. & Shafarman, W. N. Bulk and metastable defects in CuIn1−xGaxSe2 thin films using drive-level capacitance profiling. *J. Appl. Phys.* **95**, 1000–1010 (2004).

58. Nagai, T. *et al.* Characterization of Surface and Heterointerface of $Cu_2ZnSn_{1-x}Ge_xSe_4$ for Solar Cell Applications. *Phys. Status Solidi RRL – Rapid Res. Lett.* **14**, 1900708 (2020).

59. Giraldo, S. *et al.* $Cu_2ZnSnSe_4$ solar cells with 10.6% efficiency through innovative absorber engineering with Ge superficial nanolayer: $Cu_2ZnSnSe_4$ solar cells with 10.6% efficiency. *Prog. Photovolt. Res. Appl.* **24**, 1359–1367 (2016).

60. Giraldo, S. *et al.* Study and optimization of alternative MBE-deposited metallic precursors for highly efficient kesterite CZTSe:Ge solar cells. *Prog. Photovolt. Res. Appl.* **27**, 779–788 (2019).

61. Ould Salem, M. *et al.* Over 10% Efficient Wide Bandgap CIGSe Solar Cells on Transparent Substrate with Na Predeposition Treatment. *Sol. RRL* 2000284 (2020) doi:10.1002/solr.202000284.

62. Cuevas, A. The Recombination Parameter J0. *Energy Procedia* **55**, 53–62 (2014).

63. Li, J. *et al.* 10% Efficiency Cu2ZnSn(S,Se)4 thin film solar cells fabricated by magnetron sputtering with enlarged depletion region width. *Sol. Energy Mater. Sol. Cells* **149**, 242–249 (2016).

64. Vidal-Fuentes, P. *et al.* Efficient Se-Rich Sb_2Se_3/CdS Planar Heterojunction Solar Cells by Sequential Processing: Control and Influence of Se Content. *Sol. RRL* **4**, 2000141 (2020).

65. Nagaya, K. *et al.* Very small tail state formation in $Cu_2ZnGeSe_4$. *Appl. Phys. Lett.* **113**, 093901 (2018).

66. Xie, H. *et al.* Impact of Na Dynamics at the $Cu_2ZnSn(S,Se)_4$/CdS Interface During Post Low Temperature Treatment of Absorbers. *ACS Appl. Mater. Interfaces* **8**, 5017–5024 (2016).

67. Ojeda-Durán, E. *et al.* CZTS solar cells and the possibility of increasing VOC using evaporated Al2O3 at the CZTS/CdS interface. *Sol. Energy* **198**, 696–703 (2020).

68. Nadenau, V., Rau, U., Jasenek, A. & Schock, H. W. Electronic properties of CuGaSe2-based heterojunction solar cells. Part I. Transport analysis. *J. Appl. Phys.* **87**, 584–593 (2000).

69. Turcu, M., Pakma, O. & Rau, U. Interdependence of absorber composition and recombination mechanism in Cu(In,Ga)(Se,S)2 heterojunction solar cells. *Appl. Phys. Lett.* **80**, 2598–2600 (2002).

70. Scheer, R. Activation energy of heterojunction diode currents in the limit of interface recombination. *J. Appl. Phys.* **105**, 104505 (2009).

71. Halim, M. A. *et al.* A comparative study on charge carrier recombination across the junction region of $Cu_2ZnSn(S,Se)_4$ and $Cu(In,Ga)Se_2$ thin film solar cells. *AIP Adv.* **6**, 035216 (2016).

72. Wang, K. *et al.* Thermally evaporated Cu2ZnSnS4 solar cells. *Appl. Phys. Lett.* **97**, 143508 (2010).